2010 IEEE/ASME International Conference on
Advanced Intelligent Mechatronics
Montréal, Canada, July 6-9, 2010

Explicit Finite Element Analysis of a Flexible Multibody Dynamic System with Highly Damped Compliant Fingers

Chih-Hsing Liu and Kok-Meng Lee, *Fellow, IEEE/ASME*

***Abstract*– Many industries require transferring objects from conveyors to a processing line at production rate. In food processing, grasping mechanisms with highly damped compliant fingers must be capable of accommodating a limited range of object shapes/sizes without causing damages on the products being handled. Most existing models, however, are inadequate to predict the dynamics of a compliant mechanism with large deformation, contact nonlinearity, and complex 3D geometries. This paper investigates the explicit finite-element (FE) method for industrial automation applications, where both geometric and operational parameters must be evaluated. Specifically, this paper discusses the effects of several key factors (that include material properties and element types as well as the numbers of nodes) on a FE computation. Along with an experiment /computation method (that relaxes limitations of a log-decrement method generally valid for systems with an oscillatory response), the procedure to account for the damping effect in simulating the dynamics of a compliant grasping system is numerically illustrated with experimental validation against published data.**

Index Terms – flexible mechanism, robotic hand, compliant finger, finite element, multibody dynamics, damping

I. Introduction

Compliant mechanisms transfer force, motion and energy through elastic deformations offering several advantages in food-product handling where designs must accommodate a limited range of object sizes/shapes. Most analyses of compliant mechanisms base primarily on pseudo-rigid-body models [1][2], which treat flexible members as rigid links with torsional pin-joints to approximate the force-deflection relationship. However, these existing models are often inadequate to analyse the dynamic performance of a compliant mechanism with large deformation, contact nonlinearity, and complex 3D geometries.

This paper has been motivated by the needs to develop simulation techniques for designing an automated live bird transfer system (LBTS) [3] to handle live products from conveyors to a production line for meat processing. One of its fundamental tasks is the design/control of a compliant grasping mechanism where compliant fingers are an ideal candidate for this application. As compared to mechanical fingers with rigid elements connected by multiple active joints, compliant fingers have many advantages including lightweight, no relative moving parts, less expensive to manufacture; more importantly, its flexibility to accommodate a limited range of sizes/shapes and natural reactions without causing damages on the products makes them an attractive candidate for use in high-speed production.

Designing an effective motion controller of a LBTS requires a good understanding of the object dynamics throughout the grasping process. Furthermore, it is desired to minimize the number of live birds used in the experiments. In addition, the ability to predict bird motion will help reduce the number of hardware/software design configurations to be tested and prototyping cycle time. Yin and Lee [4] extended their earlier work [5] on 2D models of a flexible finger to analyse the grasping dynamics of a bird. Several improved analytical models [6][7] to predict the contact force and deflected shape of the compliant fingers have been developed. These studies generally modelled the finger as a 2D beam, and analysed the finger dynamics quasi-statically without considering the damping effect.

Finite element analysis (FEA) has been increasingly used to analyse dynamic systems; for example, impact and penetration analysis of fuselage-like structures [8], crash simulation of automobiles [9][10], and bird-strike simulation of aeronautic structures [11]. Dynamic FEA (that reduces physical tests and design cost/time) involves time-integration which can be broadly classified into two categories; implicit and explicit methods. Implicit methods are stable for linear and many nonlinear problems but computationally more expensive than an explicit method since the latter does not require stiffness matrix inversions. However, explicit methods are only stable when the time-step is limited by the Courant-Friedrichs-Levy (CFL) condition [12] [13].

Fig. 1 compares two parameter-evaluations in a typical design of a compliant multibody dynamic system (CMDS). Most FEA evaluates geometrically (size and shape) under stress and/or displacement constraints (Fig. 1a). For industrial automation, synchronization of speeds among processes under trajectory constraints (Fig. 1b) requires evaluation of operational parameters. Inertia and damping terms must be considered when solving dynamic problems. For a CMDS, both geometric and operating parameters must be evaluated during design. In addition, damping effects essential for realistic simulations are often neglected or given some presumed values. To obtain the damping parameters, time or frequency domain experiments are usually required; for examples, free vibration of steel poles and tubular towers measured by accelerometers [14]; impulse response of a wire cable [15] captured using high-speed camera; and frequency response of a gearbox [16] measured with a laser vibrometer.

Manuscript received February 14, 2010. This work was supported in part by Georgia FoodPAC and FIP programs.
Chih-Hsing Liu and Prof. Kok-Meng Lee are with the George W. Woodruff School of Mechanical Engineering, Georgia Institute of Technology, Atlanta, GA 30332-0405, USA(e-mail: kokmeng.lee@me.gatech.edu).

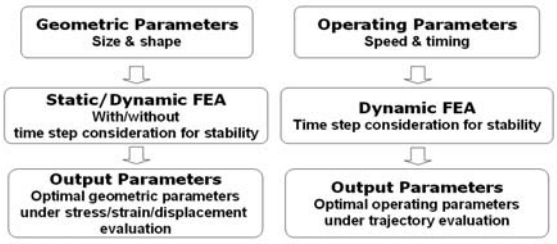

(a) Geometric parameters (b) Operating parameters

Fig. 1 Comparison of two FEA-based parameter-evaluation procedures

In the context of a practical application, this paper investigates the explicit-FEA method for analysing a CMDS with highly damped fingers, and offers the following:

- Parametric effects on computation time are discussed, which include material properties and element types as well as the numbers of elements and nodes.
- A coupled experiment/computation method to account for the damping effect is illustrated, which relaxes some limitations in traditional methods generally valid for systems with an oscillatory response.
- Computed results have been experimentally validated against published data.

II. FEA-BASED MODEL FOR AUTOMATION APPLICATIONS

The discrete equations of motion for FEA can be derived from the work balance contributed by the external load, inertial and viscous effects, and strain energy as outlined in Appendix A. ANSYS and LS-DYNA (with a built-in penalty method to handle deformable contacts) are used here to create the discrete domain $\{X\}$ and solve (A.4) using the explicit FEA method respectively.

A. Computational Time Consideration

Explicit FEM determines the next time-step unknowns in terms of previously computed quantities. While computationally efficient, it requires the time step Δt to satisfy (1) to ensure numerical stability [12] [13]:

$$\Delta t \le 2/\omega_{\max} \quad \text{where } \omega_{max} = \text{highest natural frequency} \qquad (1)$$

The critical time-step Δt_c depends on material properties and element size/shape. As an illustration, consider the formulation of a 1D un-damped rod (density ρ, elastic modulus E, cross-sectional area A). Assigning lumped masses (at the nodes), the characteristic equation can be written in the matrix form:

$$\det([K]-\omega^2[M])=0 \qquad (2)$$

where $[K]=\frac{AE}{L_e}\begin{bmatrix}1 & -1\\ -1 & 1\end{bmatrix}$; $[M]=\frac{\rho AL_e}{2}\begin{bmatrix}1 & 0\\ 0 & 1\end{bmatrix}$; and

L_e is the element length for this 1D problem. Equation (2) implies $\omega_{\max}=2c_w/L_e$ where the wave propagation speed is $c_w=\sqrt{E/\rho}$. From (1) the CFL condition is given by (3):

$$\Delta t \le \Delta t_c = L_e/c_w \qquad (3)$$

In other words, Δt must be sufficiently small that the wave does not propagate across more than one element.

As elements deform, Δt must be calculated at each time step and for each element, (Δt_i, $i=1\sim n$, n is element number). For stability considerations, the smallest time-step in the global domain is scaled by a (between 0 and1):

$$\Delta t_{num} = a \times min\{\Delta t_1, \Delta t_2, \ldots \Delta t_n\} \qquad (4)$$

In this paper, a=0.9. Δt_c depends on element (type, size, shape) and material properties and is formulated in Table 1, where L_i is the length of the sides defining the shell element; Q is a function of the bulk viscosity coefficients C_0 and C_1; $\dot{\varepsilon}$ is the strain rate; V_e is the element volume; and A_{emax} is the area of the element with a largest side.

Table 1: Critical time step formulations

Element	Δt	c_w	L_e
Beam	L_e/c_w	$\sqrt{E/\rho}=c_b$	*element length*
Shell	L_e/c_w	$c_b/\sqrt{(1-\upsilon^2)}$	$L_e=A/L_{\max}$
	Quad: $L_{\max}=\max(L_1,L_2,L_3,L_4)$; Tri.: $L_{\max}=\max(L_1,L_2,L_3)/2$		
Solid	$\frac{L_e}{Q+\sqrt{(Q^2+c_w^2)}}$	$\sqrt{\frac{(1-\upsilon)}{(1+\upsilon)(1-2\upsilon)}}C_b$	$Q=\begin{cases}C_1c_w+C_0L_e\lvert\dot{\varepsilon}_{kk}\rvert, & \dot{\varepsilon}_{kk}<0\\ 0, & \dot{\varepsilon}_{kk}\ge 0\end{cases}$
	Hexa.: $L_e=V_e/A_{\max}$; Tetra.: L_e= *minimum altitude*		

Table 2 compares three types of elements (triangular and quadrangular with two different aspect ratios), their critical time-steps, and the number of steps needed to solve a 1-ms dynamic problem for each type of elements. For the same L_1, Quad 1 requires the smallest number of steps to solve a 1ms problem. Table 2 suggests that uniform mesh with regular quadrangular (or hexahedral solid) elements are preferred for computational efficiency. In addition, Δt_c which increases linearly with the characteristic length implies that FE mesh must be carefully planed. Provided that accuracy requirements are met, smaller elements should be avoided. A general discussion of critical time-steps for different element types can be found in [17].

Table 2 Effect of element size/shape on critical time step

Elements	Triangular	Quad 1	Quad 2
Shape	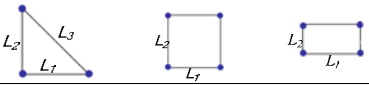		
L_2/L_1	1	1	0.5
L_e/L_1	0.71	1	0.5
Δt_c (μs)	1.32	**1.87**	0.93
Steps for 1ms computation	758	**535**	1070

Parameters: L_1=10mm; c_w=5355m/s, Material: E=69GPa; ρ=2700 kg/m^3; υ=0.33

Table 3 and the graphical illustration in Fig. 2 show the effects of material properties and characteristic length on Δt_c calculations. A higher E or a lower ρ results in smaller Δt_c. An effective way to increase Δt_c is to scale the density (and hence the mass) of some smallest elements; as long as the increased mass is significantly small compared to the overall mass, its effect on the global dynamics can be neglected.

Table 3 Parametric values used in time-step study (L_1=10mm, Quad 1)

Parameters	E (GPa)	ρ (kg/m^3)	L_e/L_1	υ
Elastic module E	**[10, 500]**	2700	1	0.3
Density ρ	70	**[100, 5,000]**	1	0.3
Char. Length L_e	70	2700	**[0.1, 2.5]**	0.3
Poisson ratio υ	70	2700	1	**[0, 0.5]**

B. *Damping Model Consideration*

In this paper, Rayleigh damping is assumed:

$$[C] = \alpha[M] + \beta[K] \tag{5}$$

where the mass and stiffness matrices, [*M*] and [*K*] defined in (A.4), can be formulated once the element types are defined. In (5), the relative effect of the coefficients α and β on the damping ratio ζ can be illustrated with a classical single-DOF system (mass *m*, spring *k* and damper *c*), where the natural frequency ω_n and damping ratio ζ are written as

$$\omega_n^2 = k/m \text{ and } \zeta = c/c_{cr} = (\alpha/\omega_n + \beta\omega_n)/2 \tag{6a,b}$$

Fig. 3 plots (6b) as a function of ω_n showing the α-term dominates in low frequency (mode) applications.

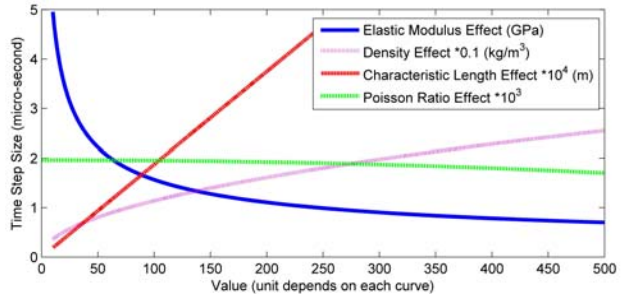

Fig. 2 Parameter-effects on critical time-step

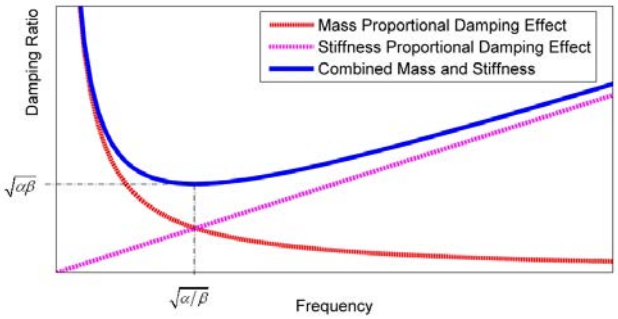

Fig. 3 Relative effect of proportional damping on damping ratio

For low-frequency continuum structural applications, the stiffness proportional damping (β-term) can be neglected, and the coefficient α is determined using a coupled experiment/computation technique (Fig. 4). As illustrated in Fig. 4, the method numerically searches for the critical α value (α_{cr}) between oscillation and non-oscillation responses, and the α value such that the solution to (A.4) agrees with the experimentally obtained impulse response.

III. Design Procedure with Illustrative Example

Figure 5 illustrates the iterative procedure for design of a CMDS, where the geometry model can be built using general CAD (or CAE) packages to serve as a FEA model. The FEA-based design process takes into account the effect of time-step size (a compromise between numerical stability and computation in explicit-dynamic FEA), mode shapes, damping model and optimized topology on the dynamic performance. As shown in Fig. 5, the input parameters is evaluated iteratively until the dynamic response meet the design requirements, which leads to a set of optimum parameters for operating the flexible multi-body system.

The design procedure is illustrated in the context of a practical application (Fig. 6), where live broiders (meat chickens) are transferred from conveyors to a production line. Simulations play an important role to reduce the number of tests on live products [5]. The values of the parameters (Fig. 6 and Table 4) in this numerical investigation are based on published designs [4] [5] so that results can be validated.

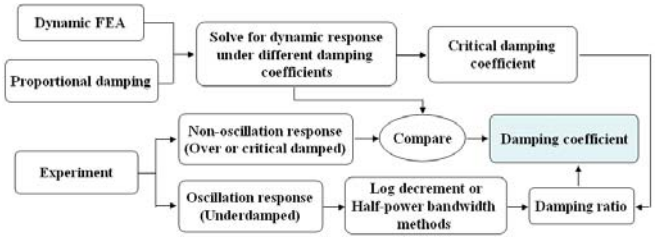

Fig. 4 Coupled computation/experiment method for damping identification

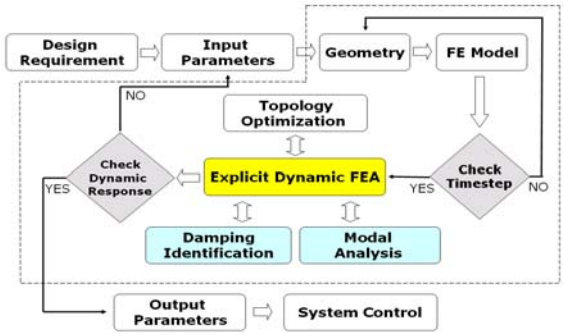

Fig. 5 Illustrative design procedure of a CMDS

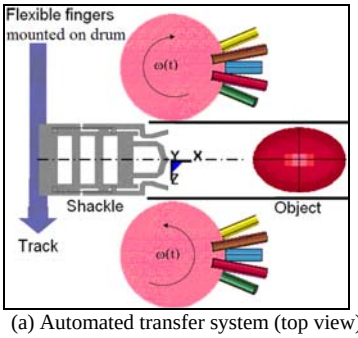

(a) Automated transfer system (top view)

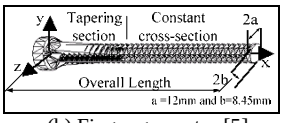

(b) Finger geometry [5]

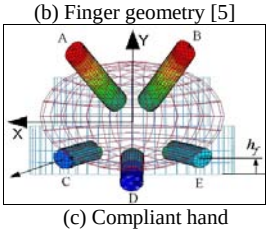

(c) Compliant hand

Fig. 6 Automated transfer system with compliant fingers

Fig. 6(a) is a plan view of an automated LBTS consisting of a conveyor on which singulated birds are transported, body-grasper made up by a pair of mechanical hands (with compliant fingers), and shackling mechanism with a pair of leg-grippers. A typical cycle begins with the bird moving towards the "hands" (rotating towards each other at an angular velocity ω). While the bird body is being cradled between the mechanical hands, both shanks of the bird are guided into the leg-grippers of the inclined shackle. A cam mechanism then rotates the shackled bird about the Y-axis out of the grasping area while inverting its body about the Z-axis for subsequent processing. Among the requirements are that live birds must be handled at a specified production rate without causing damages. In this CMDS example, the operational parameters are the angular velocity of the rotating hands with respect to the conveyor.

Table 4: Finger geometry and layout [4]

Finger #	**A**	**B**	**C**	**D**	**E**
Length (mm)	114		76		
Base location (mm)					
Drum radius	83			108	
Height, h_f	76.2		25.4	19	25.4
Orientation (°)					
Global Y-axis	–11.25	11.25	–22.5	0	22.5
Finger x-axis	45	–45	–45	0	45
Finger z-axis	10	10	–2.5	–10	–2.5

The key components here are the rotating compliant fingers. Meshed by 10-node tetra element (SOLID92 in ANSYS) with totally 83721 nodes and 53349 elements, the mode shapes of an 8-inch compliant finger (manufactured by the Waukesha Rubber Company) were numerically extracted from FEM using the Block Lanczos method. Fig. 7 shows the first 5 mode-shapes and their natural frequencies (corresponding to the square root of the stiffness-to-mass ratio); a lower frequency implies a lower stiffness in free vibration Most of the first 10 mode-shapes correspond to bending deformation except the 5th (45.8Hz) and 10th (132.9Hz) modes are torsional, and 9th mode (100.5Hz) is in elongation. The CMDS is designed such that the fingers are employed in the 1st mode which is thus the target mode for modelling the damping effect.

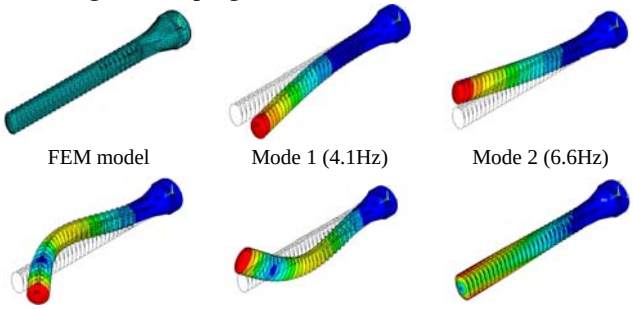

FEM model | Mode 1 (4.1Hz) | Mode 2 (6.6Hz)

Mode 3 (21.8Hz) | Mode 4 (37.1Hz) | Mode 5 (45.8Hz)

Fig. 7 First five mode-shapes of the 8-inch compliant finger

The coupled experiment/computation approach for identifying the damping coefficient, though straight-forward, is computationally time consuming. To reduce computation to an acceptable level, three simplified FE models (denoted as SM-A, B and C in Table 5) are compared against the detailed model. All three simplified models have constant elliptical cross-sections but different element sizes and/or shapes. Simulated tip responses and maximum equivalent stresses of the compliant finger using (5) to an impulse load (with α=180s^{-1} β=0) are compared in Fig. 8. Some observations can be made from Table 5:

1) Since tetra's need a smaller time step than hexa's for the same average length, SM-C (Tetra) requires 3.21 times more steps than SM-A (Hexa) in computing a 0.2s problem. Also, SM-C has a larger average element length than SM-B (Refined Hexa) but needs a smaller time-step.

2) DM cannot be meshed with hexa elements because of its complex geometry. Small detailed features lead to relatively non-homogeneous element lengths. As the time step is determined by the smallest element in the whole domain, this leads to a large number of steps (around 18.36 times than SM-A to solve the same 0.2s problem.

3) Since the matrix size is $3n\times3n$ where n is the number of nodes for each time step, the actual computational time ratios of SM-B and SM-C (relative to SM-A) are expected to be even larger than the step ratios.

4) SM-A, B and C yield similar tip responses and stress curves as seen in Figs. 8(a) and 8(b). DM (with ribs and stronger fixed end) is stiffer than the simplified models.

For the same α of 180s^{-1}, the simplified models exhibit an over-damped response while the detailed model appears under-damped. This is because their geometries are different, and thus their mass and stiffness matrices. The detailed model with α=260s^{-1} gives a similar over-damped tip response but estimate a lower stress curve than the simplified model. In other words, SM-A (that can be computed with a largest time-step) overestimates the deflection/stress than the detailed model and thus, it represents a more conservative model will be used in the following dynamic simulation.

Table 5 Different FEM models of a 4.5-inch compliant finger

FEM Models Rubber E=6.1 MPa υ=0.49 ρ=1000 kg/m^3		**Element** Type Average length # of nodes # of elements	**Numerical Time Step** Step size (μs) # Steps to 0.2s # of steps (step ratio relative to SM-A)
Detailed Model (DM)		**Tetra** 2.8mm 36782 23147	0.22 909091 18.36
Simplified Model A (SM-A)	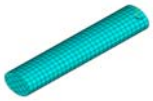	**Haxa** 4 mm 1080 725	4.04 49505 1
Simplified Model B (SM-B)		**Refined Hexa** 2 mm 5900 4698	1.43 139860 2.83
Simplified Model C (SM-C)		**Tetra** 4 mm 7481 4682	1.26 158730 3.21

Table 6 Damping identification of compliant fingers

Finger Length (inches)	α_{cr} (s^{-1})	α (s^{-1})	Responses
3	350	600	Overdamped
4.5	160	180	Overdamped
6	90	15	Underdamped
8	50	7.5	Underdamped

The dynamic response of the finger was experimentally measured. With one end clamped and a (4mm-radius 1.65mm-thick) cylindrical permanent magnet attached at the free-end, the tip motion (to an applied impulse load at the free-end) was measured by a Banner S18MB magneto-resistive sensor. Figure 8(c) illustrates simulated responses of a 4.5-in finger (with five different α values; 70, 120, 160, 180 and 200). By trials and errors, α for two fingers (3-in and 4.5-in) were determined to be 600s^{-1} and 180s^{-1} respectively. With these values, Fig. 9(d) compares the SM-

A simulated the tip response of the tip against experimental data. The experiment/computation was repeated for the 6-in and 8-in fingers; results are summarized in Table 6.

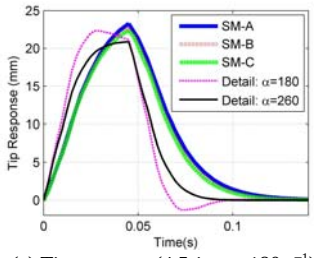

(a) Tip response (4.5-in, α=180 s^{-1})

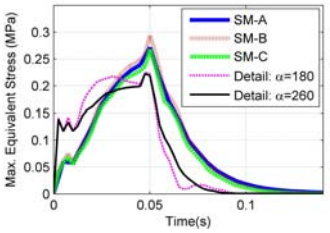

(b) Max. stresses (4.5-in, α=180 s^{-1})

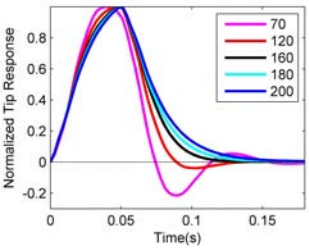

(c) 4.5-in finger response, different α

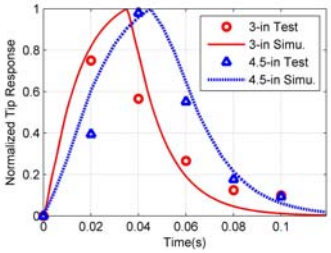

(d) 3/4.5-in fingers: α= 600/180 s^{-1})

Fig. 8 Damping Model of compliant fingers

IV. Results and Discussion

The LBTS setup (Figs. 6 and 10) was numerically analyzed, where experimental results from encoder readings and selected video clips are available [4] for validation. As in [4], the football was initially placed on the pallet moving at 0.457m/s (18in/s) towards the rotating hands. Once the pallet reached X=0.142m (5.6inches), it decelerated to 0.254m/s (10 in/s) while both robotic hands began to rotate from its initial position (Fig. 6a) at the same speed but in opposite direction. The following assumptions are made:

1) The football is a homogeneous solid with density calculated from the weight divided by volume.
2) The football is transported along the centerline and thus, a half-symmetric model is used in the simulation.
3) The football and rubber fingers are all rubber materials. The static and dynamic friction coefficients [5] between them are 0.4 and 0.3 respectively.
4) All motions follow step commands and the effects of acceleration and deceleration as in Fig. 9(a) are neglected.

Other values used in the simulation are summarized in Tables 7 and 8. The results are given in Figs. 10 and 11.

Fig. 10(a) simulates the Y-displacement of the football (using SM-A model), which agrees well with the published data, and selected snap shots as in Fig. 9(b-d) showing the instants at trapping, grasping and releasing. Fig. 10(b) simulates the X-displacement of the football relative to the pallet and maximum stress of the football. Contact locations of the fingers are illustrated in Fig. 11. The tip responses and maximum stresses on the fingers are given in Fig. 11(b-c). Both simulation and experimental results show that the compliant grasper successfully lifts the football off the pallet surface, and the duration of the lift (>5mm) is about 1 second. The simulation, however, estimates a larger maximum (about 2mm) displacement than experimental data. This discrepancy may be contributed by the following causes: 1) The simplified FE model (SM-A), which neglects the rigs and the taper fixed-end section, tends to predict a larger deflection and higher stresses. 2)The numerical simulation also ignores the effects of the acceleration of the rotating fingers and deceleration of the pallet, which contribute to some uncertainties in the actual initial contact between the football and Finger A. Experiment data offer a more uniform lift than simulation, because the football compliance is neglected. As simulated in Fig. 11, Fingers B and E bear the largest contact load (and duration). As the football was released and out of the finger contact after 2 seconds, the maximum stress on the football occurs as soon as the football is released and strikes the pallet.

Table 7 Values used in the simulation

Parameters	Values	Constraints
Football:		Drum: DOF UY =0
(Maj×Min×L) mm	(244×132×132)	
Weight (kg)	0.425	Drum center line: all DOF=0
Initial (X,Y,Z) mm	(685.5, 50.8, 184)	
Conveyor (pallet):		Ellipsoid symmetric plane: DOF UZ=0
Speed, m/s	$=\begin{cases}0.457,\ 0\le t<1.19s\\0.254,\ 1.19\le t<3s\end{cases}$	Static/dynamic friction coefficient=0.4/0.3 [4]
Pallet (L×W) mm	(200×50)	
Robotic hands:		
Finger layout	Fig. 6 and Table 4	
Speed, rpm	20, $0.75\le t\le 3s$	

Table 8 Material and element types

Parts	Material	*E* (GPa)	υ	ρ (kg/m^3)	Element Type	Element#; Node#
Football	Rubber	0.0061	0.49	275	Solid 164	512; 677
Drums	AL6061	69	0.33	2700	Shell 163	1271; 1212
Pallet	Steel	210	0.28	7700	Shell 163	2; 6
Fingers	Rubber	Solid 164	Fingers A, B: 725 elements/1080 nodes. Fingers C, D, E: 500 elements/756 nodes			

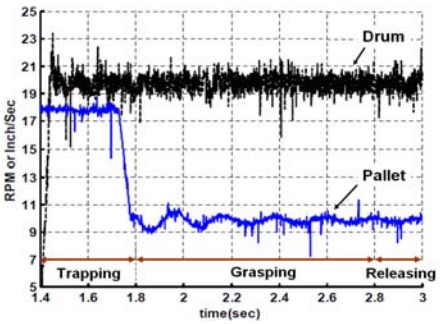

(a) Experimental obtained velocity profiles

(b) Trapping

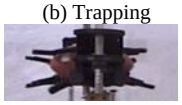

(c) Grasping

(d) Releasing

Fig. 9 Experiment of football grasping [18]

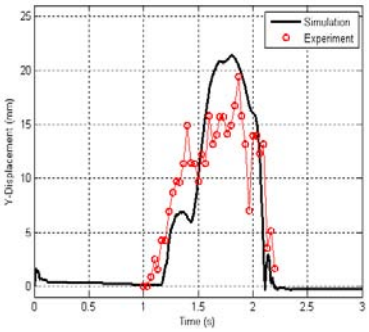

(a) Y-displacement of the football

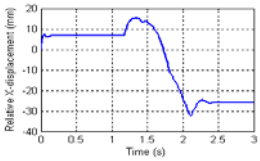

(b) Football X-disp. wrt pallet

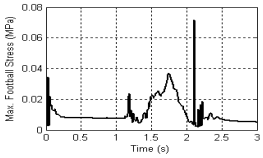

(c) Max. stress on the football

Fig. 10 Simulated responses of the football

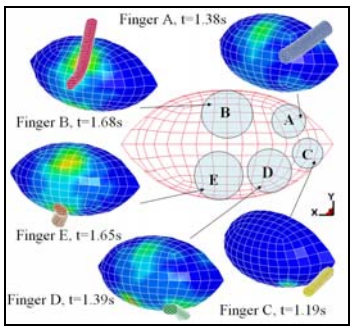

(a) Fingers/football contact regions

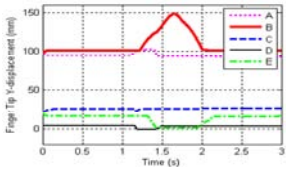

(b) Finger-tip responses (y-axis)

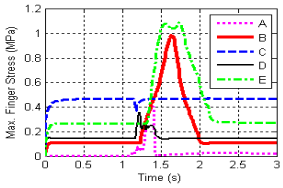

(c) Max. finger stress

Fig. 11 Simulated responses of the fingers

V. Conclusion

A practical application of an explicit FEM has been investigated for object transferring applications using ANSYS and LS-DYNA with a built-in penalty method to handle deformable contacts. A coupled experiment/ computation technique has been introduced to account for the damping effects of the rotating compliant fingers on the grasping dynamics, and experimentally validated against published data, which qualitatively agree. This paper also offers insights to the key factors (that includes material properties, element types, and node number) on computation time in terms of CFL stability condition. Although it has been illustrated in the context of an example, the procedure presented here can be used to solve a wide spectrum of compliant multibody dynamic problems with large deformable contact without neglecting the damping effects. The results also offer a better understanding of the compliant system dynamics as well as will serve as a reference for their future designs.

Appendix A: Formulation of Dynamic FEM

For a single-element subject to the body force $\{f\}$, surface traction $\{\tau\}$ and concentrated load $\{p\}$, the work balance on the element (with volumeΩ, surfaceΓ, density ρ and viscous damping coefficient c) is given by (A.1):

$$\int_\Omega \hat{u}^T\{f\}dv + \int_\Gamma \hat{u}^T\{\tau\}ds + \sum_{i=1}^{n} \hat{u}_i^T\{p\}_i = \int_\Omega \left[\hat{u}^T\rho\{\ddot{u}\} + \hat{u}^T c\{\dot{u}\} + \{\delta\varepsilon\}^T\{\sigma\}\right]dv \qquad \text{(A.1)}$$

where $\hat{u} = \{\delta u\}$; In (A.1), the right-hand side accounts for the effects due to inertia, viscosity and strain energy respectively; and $\{\delta u\}$ and $\{\delta\varepsilon\}$ are the virtual displacement and its corresponding strain.

In FE formulation where physical phenomena are analysed in discrete domains, the displacement $\{u\}$ in (A.1) is a function of space and time, and represented by interpolating functions and nodal DOF, $\{u\} = [N]\{x\}$ where $[N]$ is a space-dependent interpolation function matrix based on the element types; and $\{x\}$ is the nodal DOF dependent on time only. Using the constitutive equations

$$\{\varepsilon\} = [B]\{x\}\ ;\ \{\sigma\} = [E]\{\varepsilon\} = [E][B]\{x\} \qquad \text{(A.2a,b)}$$

where $[B]$ and $[E]$ are the strain-displacement and stress-strain matrixes. (A.1) can be written in terms of external load $\{r_{ext}\}$, and element mass, damping and stiffness matrices (respectively denoted as $[m]$, $[c]$ and $[k]$):

$$[m]\{\ddot{x}\} + [c]\{\dot{x}\} + [k]\{x\} = \{r_{ext}\} \qquad \text{(A.3)}$$

where $[m] = \int_\Omega \rho[N]^T[N]dv\ ;\ [c] = \int_\Omega c[N]^T[N]dv\ ;\ [k] = \int [B]^T[E][B]dV$;

$$\{r_{ext}\} = \int_\Omega [N]^T[f]dv + \int_\Gamma [N]^T\{\tau\}ds + \sum_{i=1}^{n}\{p\}_i \ .$$

The computational model for the system can be derived by assembling (A.4) over the whole domain to be analyzed:

$$[M]\{\ddot{X}\} + [C]\{\dot{X}\} + [K]\{X\} = \{F\} \qquad \text{(A.4)}$$

where $\{X\}$ is the global nodal DOF; $\{F\}$ is the load vector; and $[M]$, $[C]$, and $[K]$ are the global mass, damping, and stiffness matrices respectively. For a given geometries and material properties, (A.4) can be numerically modelled using a FEA package, and analysed for a given set of initial and boundary conditions using an explicit-time-integration solver.

For dynamic problems involving deformable contact, the load vector {F} in (A.4) includes contact forces at the contact interface. The interaction between two bodies (ΩA and ΩB, bounded by the boundaries ΓA and ΓB respectively) is handled as a constraint that the two bodies cannot penetrate into each other) using the penalty method [17].

References

[1] Howell, L. L., A. Midha, and T. W. Norton, "Evaluation of Equivalent Spring Stiffness for Use in a Pseudo-Rigid-Body Model of Large-Deflection Compliant Mechanisms," *ASME J. of Mechanical Design*, vol. 118, 26-131, 1996.

[2] Midha, A., L. L. Howell and T. W. Norton, "Limit Positions of Compliant Mechanisms Using the Pseudo-Rigid-Body Model Concept," *Mechanism and Machine Theory*, vol. 35, 99-115, 2000.

[3] Lee, K.-M., "Design Criteria for Developing an Automated Live-Bird Transfer System," *IEEE Trans. on Robotics and Automation*, vol. 17(4), 483 – 490, 2001.

[4] Yin, X. and K-M. Lee, "Modeling and Analysis of Grasping Dynamics for High Speed Transfer of Live Birds," *Proc. of the 2nd IFAC Conf. on Mechatronic System.* California, Dec. 9-11, 2002.

[5] Lee, K-M., J. Joni, and X. Yin, "Compliant Grasping Force Modeling for Handling of Live Objects," *ICRA2001,* May 21-26, Seoul, Korea, 1059-1064, 2001.

[6] Lan, C.-C. and K.-M. Lee, "An Analytical Contact Model for Design of Compliant Fingers," *ASME J. of Mechanical Design*, vol. 130. 2008.

[7] Li, Q. and K.-M. Lee, "An Adaptive Meshless Method for Modeling Large Mechanical Deformation and Contacts," *ASME Journal of Applied Mechanics*, vol. 75, n. 4, July 2008.

[8] Knight, N. F., N. Jaunky, R. E. Lawson, and D. R. Ambur, "Penetration Simulation for Uncontained Engine Debris Impact on Fuselage-Like Panels Using LS-DYNA", *Finite Elements in Analysis and Design*, vol. 36, n.2, 99-133, 2000.

[9] Consolazio, G. R., J. H., Chung and K. R. Gurley, "Impact Simulation and Full Scale Crash Testing of a Low Profile Concrete Work Zone Barrier," *Computers & Structures*, vol. 81, n. 13, 1359-1374, 2003.

[10] Kwasniewski, L., C. Bojanowski, J. Siervogel, J. W. Wekezer, and K. Cichocki, "Crash and Safety Assessment Program for Paratransit Buses," *Int. J. of Impact Eng*., vol. 36, n. 2, 235-242, 2009.

[11] Hanssen, A.G., Y. Girard, L. Olovsson, T. Berstad, M. Langseth, "A Numerical Model for Bird Strike of Aluminum Foam-Based Sandwich Panels," *Int. J. of Impact Eng.*, vol. 32, n. 7, 1127-1144, 2006.

[12] Mullen, R. and T. Belytschko, "An Analysis of an Unconditionally Stable Explicit Method," *Computers & Structures*, vol.16, n.6, 691-696, 1983.

[13] Cook, R. D., D. S. Malkus, M. E. Plesha, and R. J. Witt, *Concepts and Applications of Finite Element Analysis*, 4th Edition, Wiley, 2001.

[14] Pagnini, L. C. and G. Solari, "Damping Measurements of Steel Poles and Tubular Towers," *Eng. Structures*, vol. 23, n. 9, 1085-1095, 2001.

[15] Zhu, Z. H. and S. A. Meguid, "Nonlinear FE-Based Investigation of Flexural Damping of Slacking Wire Cables," *Int. J. of Solids and Structures*, vol. 44, n. 16, 5122-5132, 2007.

[16] Drew, S. J. and B. J. Stone, "Torsional Damping of a Back-to-Back Gearbox Rig: Experimental Measurements and Frequency Domain Modeling," *Proc. of the I. M. E. Part K: J. of Multi-Body Dynamics*, vol. 216, 157-168, 2002.

[17] *LS-DYNA Theorey Manual* (compiled by J. O. Hallquist), Livermore Software Technology Corporation, 2006.

[18] Yin, X., "Modeling and Analysis of Grasping Dynamics for High Speed Transfer of Live Birds," *Ph.D. Dissertation*, Georgia Institute of Technology, 2003.